Measurement 55 (2014) 335–342

Contents lists available at ScienceDirect

Measurement

journal homepage: www.elsevier.com/locate/measurement

A noncontact detection technique for interfacial bone defects and osseointegration assessment surrounding dental implants

H.B. Zhuang [a], M.Ch. Pan [a,b,*], J.Z. Chen [a], J.W. Wu [c], C.S. Chen [c,d]

[a] Department of Mechanical Engineering, National Central University, Jhongli, Taiwan
[b] Graduate Institute of Biomedical Engineering, National Central University, Jhongli, Taiwan
[c] Department of Dentistry, Cathay General Hospital, Taipei, Taiwan
[d] Department of Dentistry, Cathay General Hospital, Sijhih, Taiwan

ARTICLE INFO

Article history:
Received 4 May 2013
Received in revised form 25 May 2014
Accepted 29 May 2014
Available online 11 June 2014

Keywords:
Dental implant
Osseointegration
Bone defect
Noncontact measurement
Resonance frequency analysis

ABSTRACT

Dental implantation is popular treatment for edentulous and partially dentate patients. Effectively assessing interfacial bone defects and osseointegration requires considerable effort for successful implantation. This study presents the development of a noncontact detection technique that uses a loudspeaker and a noncontact cylindrical capacitive-type displacement sensor to measure and evaluate the severity and location of imperfections surrounding the bone–implant interface through resonance frequency (RF) analysis. To justify the effectiveness, both *in vitro* and *in vivo* experiments were performed. The acoustic sweep signal of a loudspeaker was used to excite models, and the vibration response signal from a displacement sensor was detected and transferred to the spectrum. The first RF values of the spectra on each model were subsequently identified and used to assess the interfacial situation. The measuring results show that the RF differences can be identified and applied to evaluate bone defects, as well as osseointegration. The proposed technique is a promising approach to aid dentists in assessing dental implant stability after surgery.

1. Introduction

Dental implants have provided support for prostheses in completely and partially edentulous patients, and have also become increasingly popular and crucial for oral rehabilitation. However, implant surgeries and treatments may fail because of the incomplete development of implant–bone interfacial osseointegration. Sound osseointegration around dental implants results in immobility and rigid fixation, which are prerequisites for a favorable long-term clinical outcome [1]. When bite force is applied to prostheses, peri-implant defects typically occur, in addition to imperfections in interfacial osseointegration.

To assess the bone–implant interface, investigators used early invasive methods to observe healing evolutions in animal skeletons [2]. However, this mode of detection damages interfacial developments, and is unsuitable for clinical measurements. Hence, follow-up studies primarily used noninvasive methods, which have been widely applied for evaluating postoperative situations. A clinical X-ray is a common method for interfacial observation. However, imperfections could not be detected because bone loss of less than 30% occurred [3]. Image quantification was also difficult. In other words, other detection methods are still required to justify the diagnostic result when radiography presents sound osseointegration.

Effective assessments of implant osseointegration and quantitative identification of interfacial defects are demanding for clinicians. This has drawn research attention to developing objective detection techniques and

* Corresponding author at: Department of Mechanical Engineering, National Central University, Jhongli, Taiwan. Tel.: +886 3 4267312.
E-mail address: pan_minc@cc.ncu.edu.tw (M.Ch. Pan).

http://dx.doi.org/10.1016/j.measurement.2014.05.039
0263-2241/

designing reliable measurement devices. Imperfect osseointegration can be identified based on bone–implant mobility. Based on this instability phenomenon, Periotest (Siemens AG, Germany) was first designed to assess implant stability by comparing mobility variations [4]. However, because the Periotest value (PTV) is strongly related to the excitation direction and location, the readings inaccurately present peri-implant tissue characteristics [5]. Hence, the applications of this apparatus in post-implantation evaluation remain limited.

Since the 1990s, resonance frequency analysis (RFA) has been applied to develop another technique for osseointegration stability evaluation. The resonance frequency (RF) value is related to the stiffness, damping, density of the vibration object, and its boundary condition. The RF measurement is also a noninvasive method. In certain experiments, Meredith et al. excited a sinusoidal force on dental implants, and measured the corresponding responses with a custom-designed L-shaped transducer mounted on the implants. They used this transducer to measure the first RF values of the implants on a rabbit tibia. Their results showed that RF variations are useful and discriminable indices for analyzing the healing degree [6,7]. Thus, a designated instrument (Osstell™, Integration Diagnostics AB, Sweden) was manufactured to assess the *in vitro* primary and *in vivo* secondary stability by using the Implant Stability Quotient (ISQ) value [8,9]. Ito et al. used screws to imitate peri-implant contact conditions on an *in vitro* model. They concluded that interfacial ISQ differences could be applied for an early diagnosis of overall osseointegration [8].

Castellini et al. proposed a noninvasive laser measurement procedure for diagnosing structural defects on human teeth. They also used this method to measure modal parameters of the cantilever beam. According to their results, the laser technique is an effective diagnostic tool for periodic teeth monitoring [10,11]. Huang et al. used a hammer–microphone set to examine peri-implant vibration in *in vitro* and *in vivo* tests. Their results showed that the first interfacial RF values were linearly related to their boundary heights and contact characteristics [12,13]. They then developed a new RFA detector that consisted of a miniature electromagnetic triggering rod and an acoustic receiver for an implant stability assessment. They performed experiments to validate the reliability and feasibility of this apparatus [14]. Hayashi et al. developed a noncontact electromagnetic device for monitoring periodontal conditions for *in vitro* models. They used urethane or formed urethane to design the bone defect area, and filled it with soft lining material for the *in vitro* model. They then used this device to measure simulated atrophic defects. According to their results, this apparatus might be capable of assessing the periodontal situation and implant stability [15].

Previous studies have applied various methods and devices to evaluate postoperative osseointegration and the bone defect. However, their findings have presented only an overall peri-implant assessment, without information concerning defect orientations and locations. To date, commercialized detectors still require enhancements in their measurement sensitivity and repeatability. To address these drawbacks, this study presents the development of a novel detection technique that is able to quantify defect severities and identify defect locations and evaluate osseointegration around implants. Hence, a noncontact excited-sensor procedure was applied to actuate a series of *in vitro* defect models in different vise-clamping heights, and to measure their corresponding first RFs. Moreover, *in vivo* tests were performed to estimate osseointegration on a rabbit tibia. The proposed technique is a promising approach for assisting in the diagnosis of clinical osseointegration and defects after surgery. Based on the detected imperfection orientations and locations, dentists can provide early treatment to repair bone defects and enhance the development of postoperative osseointegration.

2. Methods

2.1. Experimental in vitro models

To assess the defect orientation and location around the implant, a series of *in vitro* defect models were designed. Every model comprised a dental implant (diameter: 4.5 mm, length: 11 mm, titanium alloy, Astra Tech AB, Sweden) and an artificial bone block (10 mm × 10 mm × 20 mm, Solid rigid polyurethane block, SAWBONES®) that was used to simulate the alveolar bone. To imitate the boundary condition in the molar region, the gripped side of the model was clamped using a metal vise (10 N-cm torque). Fig. 1a shows that the vise-clamping and the non-vise-clamping sides respectively represent the mesial-distal (MD) and the buccal-lingual (BL) directions on the mandible model. Fig. 1b shows the definition of the defect severity. Each pair of 2 bold lines symbolizes the vise-clamping side. The Dft and the Clt side were defined as the defect and complete orientation, respectively. Six models embedded with the implant were designed to include the sound structure (Sound), one-column defects with 4 mm (A4) and 8 mm depths (A8), opposite-column defects with 4 mm (AC4) and 8 mm depths (AC8), and a circular defect (Severe).

Afterward, 6 blocks were prepared for each defect model. Six blocks were available for each of the A8 and AC4 models, and 12 blocks were available for each Sound, A4, AC8, and Severe model. The comprehensive test was performed. The model type named "A," "C," or both (*i.e.*, "AC") meant that an arc defect (approximately 90°) with a 1 mm gap had been made. The RFs of the various models in three directions (0°, 45°, and 90°) were all examined, and the defect in the non-vise-clamping side was set to 0°.

2.2. Noncontact RF measurement of the in vitro model

Before the *in vitro* test, the healing abutment (length: 5.5 mm, diameter: 4.5–7 mm, titanium alloy, Astra Tech AB, Sweden) was screwed onto the model. The fixation side of the model was clamped using a metal vise. As shown in Fig. 2, the noncontact RF measurement was then performed. The healing abutment was excited using a loudspeaker (diameter: 40 mm, depth: 18 mm, VSP-03T, AUTOBACS SEVEN). The vibration response was measured

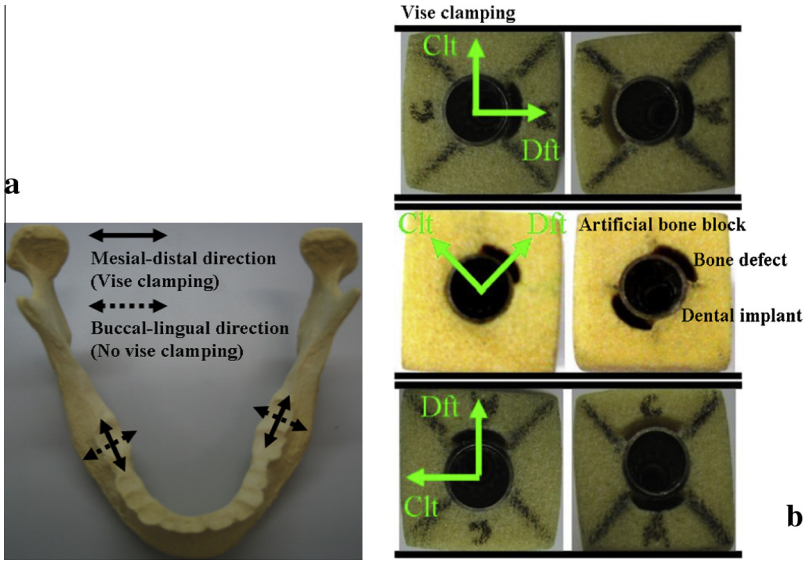

Fig. 1. (a) Mandible model with MD and BL directions illustrates the fixation condition of *in vitro* defect models, (b) where each pair of 2 bold lines represents the vise-clamping side; and (top) 0°, (middle) 45°, and (bottom) 90° defects; and (left) one-column and (right) opposite-column defects.

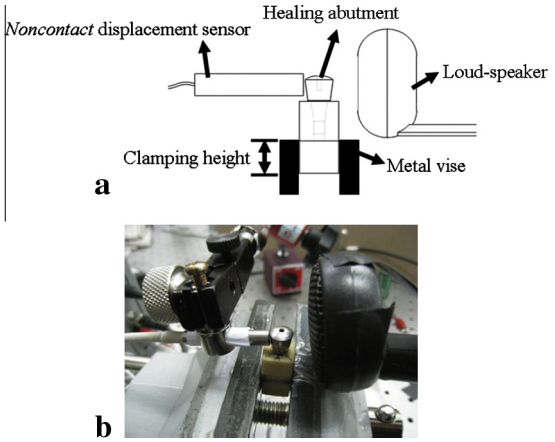

Fig. 2. Noncontact RF measurement (a and b). Four arrows indicated a noncontact displacement sensor, a healing abutment, a loudspeaker, and a metal vise. The double-headed arrow represents the clamping height.

using a noncontact cylindrical capacitive-type displacement sensor (diameter: 5 mm, length: 28 mm, range: 250 μm, C3-D, LION PRECISION).

The loudspeaker and the displacement sensor were placed opposite and separately on 2 sides of the model [16,17]. The distance between the model and the sensor situated in the effective sensing range could be confirmed by the indicator light on the sensor driver. The acoustic sweep and the vibration response signals were acquired using an I/O DSP card (SI-MOD6816-250, SHELDON INSTRUMENTS). Each model of the 2 sensing sides (Dft and Clt) and 4 clamping heights (9 mm, 10 mm, 11 mm, and 12 mm) were measured 10 times. In total, 120 data were obtained for each model (a defect type in a sensing side), except for the A8 and AC4 models, for which 60 data were obtained. In our *in vitro* (and *in vivo*) tests, we used the swept acoustic signal of a loudspeaker to excite models tested, and the vibration response detected by a displacement sensor was acquired and transferred into the spectrum. Hence we programed a user operating interface to control the I/O DSP card. The bandwidth of the swept sinusoids for excitation can be adjusted. Due to the combination of a dental implant together with both the cortical and cancellous bone, the resonance frequency of the first bending mode that most corresponds to the condition of osseointegration or defect was chosen as an index of detection, and it is noted the amplitude (or power) level on the chosen RF had no significance and was not considered in the defect detection. The mean and standard deviation of the RFs were calculated for comparison. One-way analysis of variance (ANOVA) was applied to test the relevance between each model regarding various boundary conditions and their RFs.

2.3. Noncontact RF measurements of the in vivo model

To assess the feasibility of the proposed noncontact detection technique, the *in vivo* experiment was performed. As shown in Fig. 3a and b, the standard implantation procedure was conducted by dentists. One healthy female New Zealand rabbit was used as a test subject. Two custom-made titanium implants (diameter: 3.75 mm, length: 10 mm, INTAI Corp.) with 2 healing abutments (diameter: 7 mm, length: 15 mm, INTAI Corp.) were placed in the left tibia. To investigate the benefits of the coated implants, Implant 2 differed from Implant 1 because of a surface coating.

The X-ray observation shows that the interfacial osseointegration of the tibia had developed completely after 16 weeks. Hence, the first RFs in 2 tibial directions (lateral and axial) of the tibia (Fig. 3c and d) were measured using the noncontact detection device, which consisted of a fixed

Fig. 3. Photographs of *in vivo* RF measurement. (a) Surgical implantation in a rabbit. (b) Two implants on the left proximal tibia near the femur. Their RFs were measured in the (c) lateral and the (d) axial directions.

stand, an acrylic holder, a displacement sensor, and a miniature loudspeaker (diameter: 10 mm, depth: 3.5 mm, AK-1008RA-8W, Advanced Acoustic Technology Corp.). To confirm the postoperative stability, the second RF measurement was performed 25 weeks later. The RFs of the 2 detections were recorded, yielding 15 data by using our proposed method. The mean and standard deviation were calculated. ANOVA was applied to examine the RF variations of the 2 implants in 2 measurement directions.

3. Results

3.1. In vitro bone defect measurement

The RF comparison between the Clt and the Dft sides for the various models in 3 directions and 4 clamping heights is shown in Fig. 4. Their detailed RF ranges are listed in Tables 1–3. According to the statistical results, significant differences ($p < 0.05$) were obtained for the RFs between the 2 sensing sides for all models and the clamping heights. The RFs in the Dft side were shown to be consistently smaller than those in the Clt side for the various models, in 2 directions (0° and 45°) and 4 clamping heights. However, the RFs of the Dft side in the 90° direction are higher in the presence of defects. Moreover, in the Dft side, the RFs of the various models in 3 directions and 4 clamping heights decreased significantly ($p < 0.05$) with increasing defects. However, the RFs increased significantly ($p < 0.05$) with increasing clamping heights.

3.2. In vivo osseointegration measurement

The RF comparison of the 2 implants between the lateral and axial directions on the tibia is shown in Fig. 5. The statistical results show significant differences ($p < 0.05$) in RFs of 2 implants in 2 tibial directions. The RFs in the lateral direction (1: 833 ± 8 Hz, 2: 935 ± 14 Hz) are higher than in the axial direction (1: 768 ± 11 Hz, 2: 770 ± 9 Hz). The RFs in the lateral direction for Implant 2 are higher than those for Implant 1 ($p < 0.05$). However, the RFs in the axial direction for the 2 implants have no significant difference ($p = 0.552$). Thus, the RF differences in the 2 experiments can be applied to assess interfacial defect situations (orientation, location, and severity) and osseointegration.

4. Discussion

4.1. Assessment of in vitro bone defects

To evaluate probable defect locations, the RF variations in the *in vitro* models were applied to establish an imperfection detection method. As shown in Fig. 4 and 2 RF characteristics have been determined (*i.e.*, $RF_{Dft} < RF_{Clt}$ in 0° and 45° directions, and $RF_{Dft} > RF_{Clt}$ in the 90° direction). The maximal and minimal RFs were selected from the *Sound* and *Severe* testing results. In addition, because the *Sound* and *Severe* models have 2 unclear sensing sides, the RF differences between the Dft side and the Clt side in the 45° direction are non-significant. Other models (A4, A8, AC4, and AC8) in 3 directions have obvious RF variations. Hence, the significant differences in RFs in the 2 sensing sides were employed to determine defect orientation.

After determining the defect orientation, the defect location can be evaluated by using the RF variations shown in Fig. 4. For various models in the Dft side with 3 directions and 4 clamping heights, the RFs in the 0° direction are lower than those in the 45° direction. Locations can

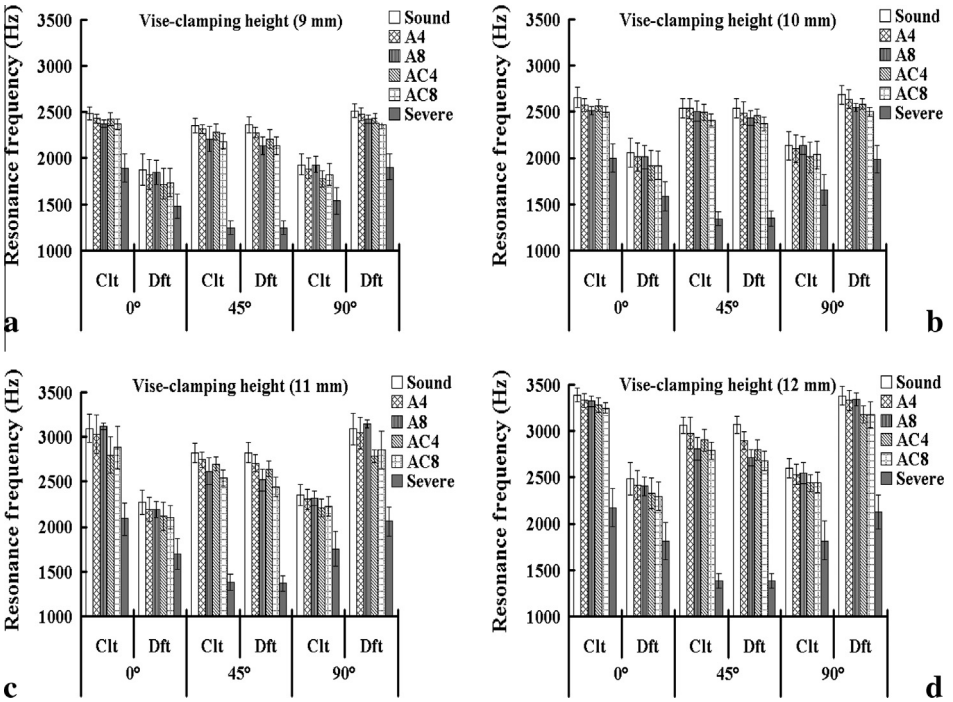

Fig. 4. RF comparison of various models and clamping heights in 2 sensing sides.

Table 1
RF range of 0° defects in the Clt and Dft sides for 4 clamping heights.

Various defect severity	RF range of 0° defects (Mean ± S.D. Hz)							
	9 mm		10 mm		11 mm		12 mm	
	Clt	Dft	Clt	Dft	Clt	Dft	Clt	Dft
Sound	2484 ± 69	1876 ± 165	2652 ± 112	2051 ± 159	3095 ± 156	2268 ± 140	3389 ± 73	2480 ± 176
A4	2429 ± 48	1826 ± 160	2570 ± 68	2009 ± 150	3027 ± 215	2187 ± 135	3329 ± 72	2412 ± 158
A8	2372 ± 37	1848 ± 127	2508 ± 45	2011 ± 124	3122 ± 37	2185 ± 90	3321 ± 56	2401 ± 103
AC4	2424 ± 70	1722 ± 164	2563 ± 66	1921 ± 158	2798 ± 206	2110 ± 160	3279 ± 77	2323 ± 164
AC8	2365 ± 59	1735 ± 150	2494 ± 58	1918 ± 148	2884 ± 240	2099 ± 133	3249 ± 60	2293 ± 150
Severe	1892 ± 150	1481 ± 134	2000 ± 149	1588 ± 157	2083 ± 180	1698 ± 172	2170 ± 203	1814 ± 196

Table 2
RF range of 45° defects in the Clt and Dft sides for 4 clamping heights.

Various defect severity	RF range of 45° defects (Mean ± S.D. Hz)							
	9 mm		10 mm		11 mm		12 mm	
	Clt	Dft	Clt	Dft	Clt	Dft	Clt	Dft
Sound	2354 ± 78	2357 ± 89	2533 ± 107	2532 ± 105	2820 ± 111	2825 ± 110	3062 ± 88	3067 ± 95
A4	2312 ± 50	2276 ± 54	2533 ± 111	2483 ± 121	2747 ± 86	2705 ± 96	2978 ± 169	2894 ± 93
A8	2205 ± 137	2131 ± 100	2502 ± 108	2429 ± 79	2616 ± 150	2518 ± 120	2804 ± 123	2708 ± 86
AC4	2279 ± 90	2205 ± 99	2492 ± 89	2454 ± 76	2698 ± 74	2644 ± 86	2900 ± 115	2794 ± 106
AC8	2177 ± 84	2133 ± 94	2407 ± 66	2365 ± 76	2539 ± 94	2443 ± 109	2788 ± 93	2673 ± 106
Severe	1249 ± 72	1250 ± 72	1346 ± 77	1350 ± 83	1379 ± 83	1367 ± 83	1386 ± 81	1388 ± 78

be discriminated using this RF difference ($RF_{0°} < RF_{45°}$). Moreover, the locations in the 90° direction can be directly determined with the preceding RF characteristic ($RF_{Dft} > RF_{Clt}$). The associated RF ranges are then applied to distinguish between defect depths. The maximal and minimal RFs respectively occur in the *Sound* and *Severe* models. In A4 and A8, the RF decrease is consistent (*i.e.*, $RF_{A8} < RF_{A4}$). Conversely, AC4 and AC8 have the same RF tendency (*i.e.*, $RF_{AC8} < RF_{AC4}$).

Because of human errors in model fabrication and measurement, in certain cases the RF variations of the Dft side (A4 and A8: 0° in 9 mm and 10 mm, 90° in

Table 3
RF range of 90° defects in the Clt and Dft sides for 4 clamping heights.

Various defect severity	RF range of 90° defects (Mean ± S.D. Hz)							
	9 mm		10 mm		11 mm		12 mm	
	Clt	Dft	Clt	Dft	Clt	Dft	Clt	Dft
Sound	1934 ± 112	2513 ± 76	2130 ± 155	2680 ± 104	2352 ± 118	3091 ± 178	2597 ± 106	3381 ± 103
A4	1888 ± 111	2476 ± 69	2094 ± 151	2632 ± 101	2302 ± 115	3043 ± 176	2530 ± 110	3329 ± 106
A8	1933 ± 82	2422 ± 42	2131 ± 94	2542 ± 46	2314 ± 85	3149 ± 46	2543 ± 115	3346 ± 70
AC4	1783 ± 89	2431 ± 54	2006 ± 164	2581 ± 57	2207 ± 98	2784 ± 75	2435 ± 94	3178 ± 91
AC8	1824 ± 113	2360 ± 47	2032 ± 142	2497 ± 51	2224 ± 106	2853 ± 216	2441 ± 108	3147 ± 139
Severe	1542 ± 145	1905 ± 135	1654 ± 167	1990 ± 145	1754 ± 191	2057 ± 160	1820 ± 207	2124 ± 186

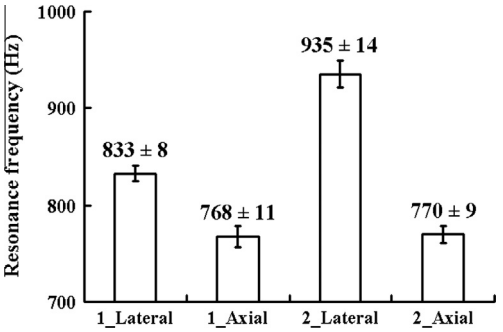

Fig. 5. RF comparison for 2 implants in 2 tibial directions.

11 mm and 12 mm; AC4 and AC8: 0° in 9 mm, 90° in 11 mm, respectively) are not apparent in Fig. 4. Nonetheless, they reach statistical significance after ANOVA testing. Therefore, the defect locations can be assessed according to these RF characteristics. Thus, as shown in Fig. 6, this study proposes a preliminary *in vitro* assessment procedure that can be used to evaluate the severity, direction, and location of peri-implant defects.

Compared with previous studies [8,15], because the mimic bone material has similar mechanical properties of the alveolar bone, the interfacial contact situation can be presented exactly after implantation. The artificial bone block was applied to simulate the appropriate cancellous bone. The clamping heights mimic and correspond to the bone quality for humans. The *in vitro* defect design belongs to the bone wall imperfection, and is consistent with clinical classification [18]. In the follow-up study, the bone envelope defect will be developed using the artificial cortical–cancellous bone block. This noncontact measurement will again be performed.

The chief cause of RF differences in the implant is the boundary conditions, such as interfacial osseointegration, the surrounding bone quality, and the exposed height of the implant. As shown in Fig. 4, RFs vary with the peri-implant defect situation and the clamping height. The exposed height of the implant increases with the defect region. The increase in clamping height represents a relative and stable bone quality. Therefore, each model shows a significant RF decrease with increasing defect regions. The RF increases invariably with the clamping height. The results show that the boundary condition (defect severity and bone quality) affects the structural stability, and can be used to assess the defect location.

For quantifying interfacial variations, impact excitation has been widely used to examine the structural RFs in dental research. A transient force with a broad-band spectrum was applied by generating impact force with a hammer, yielding a structural response with specific frequencies corresponding to the structural resonances. A primary feature of the impact technique was the use of an accelerometer attached firmly to the structure for acquiring its

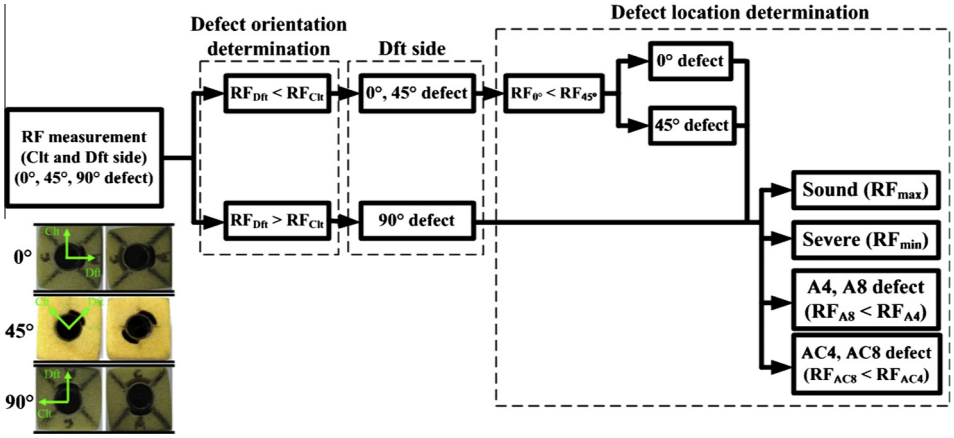

Fig. 6. Preliminary *in vitro* assessment procedure for the defect orientation and location.

response [19]. This introduces the mass loading effect, which causes the accelerometer to lower RFs, especially if the structure of the dental implant is particularly small.

Perfect hammer excitation invariably requires appropriate practices; otherwise, double hitting may introduce incorrect resonant peaks. To eliminate the loading effect, an impact rod driven by electromagnetic force was used to generate excitation [14], which eventually forms a contact force. The issue of the broadness of the spectral energy entering the implant requires further investigation. Alternatively, the authors employed a disk magnet, an acceleration sensor as the vibrator, and a detector attached directly to a cylindrical titanium rod [15]. Their method needs a contact sensor, and the loading effect remains. Our study proposes a fully noncontact excitation and sensing technique. The loudspeaker and the capacitive-type displacement sensor were used to excite and measure various models. This novel detection approach can be used to prevent the loading effect during RF measurements. The spectral band of acoustic energy excitation is tunable for individual implant-bone structures.

4.2. Assessment of in vivo osseointegration

To examine the correlation between RF variations and postoperative osseointegration, the authors in [7] demonstrated that the RFs of rabbit tibias in the parallel direction were evidently lower than those in the perpendicular direction after 14 and 28 days. As shown in Fig. 5, the experimental results of the current study are consistent with [7], and show that the coating on the implant encourages osseointegration development. However, the RF difference in the axial direction was not apparent for 2 implants. Because their distance was relatively near, the tibial destruction led to a decrease in axial implant stability. The result shows that (1) the RF in the lateral direction is larger than that in the axial direction because the cortical bone in the lateral direction near the implant facilitates stiffening, (2) the implant coating can promote interfacial strength, and (3) the rabbit tibia is unsuitable for embedding 2 implants. In other words, the proposed noncontact detection technique is feasible to be used for assessing osseointegration and monitoring prognosis stability.

5. Conclusion

This study proposed a detection procedure and presented its application to evaluate the defect orientation and location around dental implants by conducting *in vitro* RF measurements. The orientation was first determined by comparing RF differences between a defect and the complete side. The location was subsequently identified using RF variations. In the *in vivo* trial, the noncontact detection technique was used to assess interfacial osseointegration and examine the benefits of an implant surface coating. Thus, to expedite the realization of a detection device in the oral measurement, as shown in Fig. 7, the integrated excitation-and-detection transducer is proposed and composed of a pair of miniature loudspeaker and noncontact displacement sensor. In the noncontact detection, the clinical healing abutment is first connected with the implant. Then the transducer is to enclose around the abutment. During the RF measurement, the acoustic energy from the loudspeaker excites the structure, and the structural response is sensed by the displacement sensor. The first bending-mode RF value is subsequently obtained by the spectrum analysis and applied to assess various interfacial conditions upon their specific RF variation characteristics. In this procedure, the severity and orientation of osseointegration instability can be assessed. While using the device in a busy dental surgery environment, specific sound energy of swept sinusoids is applied to excite the implant structure, and vibration response is acquired by a noncontact displacement pickup. As the vibration displacements are sensed rather than acoustic signals, a promising and reliable measurement can still be anticipated. That is, the background noise at the dental surgery site, if it exists, can be part of excitation energy, and will not vary the detection result. The proposed technique can be applied to help dentists assess and remedy potential interfacial imperfections, to reduce instances of expected failure in dental implantation.

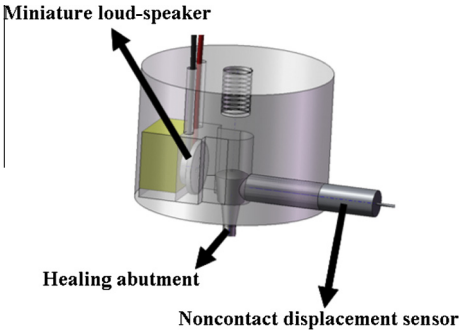

Fig. 7. Schematic diagram of an integrated excitation-and-detection transducer composed of a pair of miniature loudspeaker and noncontact displacement sensor.

Acknowledgements

This study was financially supported by grants from the Nation Science Council of Taiwan (NSC97-2221-E-008-010- MY3) and from the Cathay General Hospital of Taipei, Taiwan (98CGH-NCU-B2 and 101CGH-NCU-B2).

References

[1] P.I. Brånemark, Introduction to osseointegration, in: P.I. Brånemark, G.A. Zarb, T. Albrektsson (Eds.), Tissue-Integrated Prostheses: Osseointegration in Clinical Dentistry, Quintessence Publishing, Chicago, 1985, pp. 11–12.
[2] A. Wennerberg, T. Albrektsson, B. Andersson, J.J. Krol, A histomorphometric and removal torque study of screw-shaped titanium implants with three different surface topographies, Clin. Oral Implant. Res. 6 (1995) 24–30.
[3] S. Sundén, K. Gröndahl, H.G. Gröndahl, Accuracy and precision in the radiographic diagnosis of clinical instability in Brånkmark dental implants, Clin. Oral Implant. Res. 6 (1995) 220–226.
[4] H. Oka, T. Yamamoto, K. Saratani, T. Kawazoe, Automatic diagnosis system of tooth mobility for clinical use, Med. Prog. Technol. 16 (1990) 117–124.
[5] H. Caulier, I. Naert, W. Kalk, J.A. Jansen, The relationship of some histologic parameters, radiographic evaluations, and Periotest

measurements of oral implants: an experimental animal study, Int. J. Oral Maxillofac. Implants 12 (1997) 380–386.
[6] N. Meredith, D. Alleyne, P. Cawley, Quantitative determination of the stability of the implant–tissue interface using resonance frequency analysis, Clin. Oral Implant. Res. 7 (1996) 261–267.
[7] N. Meredith, F. Shagaldi, D. Alleyne, L. Sennerby, P. Cawley, The application of resonance frequency measurements to study the stability of titanium implants during healing in the rabbit tibia, Clin. Oral Implant. Res. 8 (1997) 234–243.
[8] Y. Ito, D. Sato, S. Yoneda, D. Ito, H. Kondo, S. Kasugai, Relevance of resonance frequency analysis to evaluate dental implant sability: simulation and histomorphometrical animal experiments, Clin. Oral Implant. Res. 19 (2008) 9–14.
[9] J. Blanco, E. Alvarez, F. Muñoz, A. Liñares, A. Cantalapiedra, Influence on early osseointegration of dental implants installed with two different drilling protocols: a histomorphometric study in rabbit, Clin. Oral Implant. Res. 22 (2011) 92–99.
[10] P. Castellini, L. Scalise, G.M. Revel, Vibration measurements for diagnosis of structural defects on human teeth, Measurement 27 (2000) 29–42.
[11] P. Castellini, G.M. Revel, L. Scalise, Measurement of vibrational modal parameters using laser pulse excitation techniques, Measurement 35 (2004) 163–179.
[12] H.M. Huang, S.Y. Lee, C.Y. Yeh, C.T. Lin, Resonance frequency assessment of dental implant stability with various bone qualities: a numerical approach, Clin. Oral Implant. Res. 13 (2002) 65–74.
[13] H.M. Huang, C.L. Chiu, C.Y. Yeh, C.T. Lin, L.H. Lin, S.Y. Lee, Early detection of implant healing process using resonance frequency analysis, Clin. Oral Implant. Res. 14 (2003) 437–443.
[14] W.J. Chang, S.Y. Lee, C.C. Wu, C.T. Lin, Y. Abiko, N. Yamamichi, H.M. Huang, A newly designed resonance frequency analysis device for dental implant stability detection, Dent. Mater. J. 26 (2007) 665–671.
[15] M. Hayashi, C. Kobayashi, H. Ogata, M. Yamaoka, B. Ogiso, A no-contact vibration device for measuring implant stability, Clin. Oral Implant. Res. 21 (2010) 931–936.
[16] H.-B. Zhuang, W.-S.h. Tu, M.-C.h. Pan, J.-W. Wu, Ch.-S. Chen, Sh.-Y. Lee, Y.-C.h. Yang, Noncontact vibro-acoustic detection technique for dental osseointegration examination, J. Med. Biol. Eng. 33 (2013) 35–43.
[17] M.-C.h. Pan, H.B. Zhuang, Ch.-S. Chen, J.-W. Wu, Sh.-Y. Lee, A noncontact resonance frequency detection technique for the interfacial bone defect assessment around the dental implant, Med. Eng. Phys. 35 (2013) 1825–1830.
[18] L. Vanden Bogaerde, A proposal for the classification of bony defects to dental implants, Int. J. Periodont. Rest. Dent. 24 (2004) 264–271.
[19] N. Meredith, A review of nondestructive test methods and their application to measure the stability and osseointegration of bone anchored endosseous implants, Crit. Rev. Biomed. Eng. 26 (1998) 275–291.